Materials Research. 2016; 19(2): 316-321
DOI:http://dx.doi.org/10.1590/1980-5373-MR-2015-0491

Positron Annihilation Spectroscopy Study on Annealing Effect of CuO Nanoparticles

Jianjian Shi[a], Jiaheng Wang[a], Wei Yang[a], Zhejie Zhu[a], Yichu Wu[a]*

[a]School of Physics and Technology, Hubei Key Laboratory of Nuclear Solid State Physics, Wuhan University – WHU, Wuhan, 430072, China.

Received: August 23, 2015; Revised: December 9, 2015; Accepted: December 17, 2015

The microstructure and defects of CuO nanoparticles under isochronal annealing were investigated by positron annihilation spectroscopy (PAS), X-ray diffraction (XRD) and scanning electron microscope (SEM). XRD and SEM results indicated that the average grain sizes of CuO nanoparticles grew slowly below 800 °C, and then increased rapidly with the annealing temperature from 800 to 1000 °C. Positron lifetime analysis exhibited that positrons were mainly annihilated in mono-vacancies (V_{Cu}, V_O) and vacancy clusters when annealing from 200 to 800 °C. Furthermore, *W*-*S* plot of Doppler broadening spectra at different annealing temperatures found that the (*W*, *S*) points distributed on two different defect species, which suggested that $V_{Cu}^{-} - V_O^{+}$ complexes were produced when the grains grew to bigger size after annealing above 800 °C, and positrons might annihilate at these complexes.

Keywords: *positron annihilation, defect, nanoparticle, CuO*

1. Introduction

Cupric oxide (CuO) is a well-known *p*-type semiconductor material with an indirect band gap of 1.0 eV[1], which has attracted a large number of studies in polycrystalline as well as single crystal of CuO by using a variety of techniques. Especially, nano-sized CuO has raised the most prospective applications over the years, such as gas sensors[2], catalysis[3, 4], supercapacitor[5, 6], ceramics[7], batteries[8], solar energy cells[9] and field emission emitters[10].

Though CuO has numerous potential applications, the lack of control over the defects is still a big problem for practical devices. It has been found that the grain surface and interface are rich of defects such as vacancies (V_{Cu} or V_O, where the subscript refers to the missing host atom), antisite defects (Cu_O or O_{Cu}, where A_B means "*B*" atom is replaced by "*A*" atom) and isolated interstitials (O_i or Cu_i). However, the high formation energies of these defects lead to an unstable state at equilibrium[11]. These defects offer a scope to tune the useful material properties through proper choice of annealing environment and temperature. The negatively charged vacancy, V_{Cu}^{2-}, where the superscript refers to the charge $q(-2)$ of the defect, is thought to be the source of CuO having *p*-type conductivity[12, 13]. Gao et al.,[14] reported that oxygen vacancies at the interface of the particles were suggested to be responsible for the ferromagnetism in the CuO nanoparticles, vacuum annealing enhanced the ferromagnetism of the CuO nanoparticles, while oxygen atmosphere annealing reduced it. Shi et al.[15] found that the tunable ferromagnetism for the Cu_2O/Cu nanoparticles composites was attributed to Cu vacancies at the interfaces.

With a large surface to volume ratio, surface effects dominate nanoparticles properties over their respective bulk features. CuO nanoparticles exhibit unique optical, electrical, and magnetic properties based on the effects of grain size and quantum dots size as the surface contribution becomes dominant[16-19]. Positron annihilation spectroscopy (PAS) has been used as a sensitive probe to characterize surface and interface defects in nanoctystalline metals[20-22] and semiconductor nanoparticles[23-25]. This is mainly due to the fact that the size of nanoparticles is much smaller than the positron diffusion length ($L_+ \sim 100$nm)[26]. Positrons are trapped at defects such as open volumes (vacancies, vacancy clusters and voids) located at the grain surface or interface. Therefore, the positron annihilation radiation parameters provide information on the microstructure of grain surfaces or interfaces. Positron lifetime annihilation parameters can be directly correlated to the size and concentration of defects at the surfaces or interfaces. Doppler broadening parameters give information about the electron momentum distribution at the annihilation site[27]. Some authors investigated defect structure of CuO nanoparticles by positron annihilation technology[28-30]. They found that there existed a large number of copper- and/or oxygen- related vacancies or complexes in CuO nanoparticles, which depended on the annealing environment and temperature. However, it should be mentioned that the feature of defects in different sizes of CuO nanoparticles is far from understood and requires extensive studies in CuO nanoparticles. In this work, the generation and recovery of defects located at grain surfaces or interfaces in CuO nanoparticles under isochronal annealing were investigated by positron annihilation lifetime and Doppler broadening spectroscopy, together with traditional XRD and SEM techniques.

2. Experimental

2.1. Sample preparation

CuO nanoparticles with a size of about 40 nm were purchased from Beijing dekedaojin High Technology Ltd, China with a purity of 99.9%. The nanoparticle powders

*e-mail: ycwu@whu.edu.cn

were hand milled for 2 h in an agate mortar with a pestle and then pressed into pellets (diameter: 15 mm, thickness: 1 mm) under a static pressure of about 10 MPa for 5 min at room temperature. The annealing experiments were made over a temperature range in the stable region of the CuO phase, i.e. $T < 1027$ °C[1, 31]. So, the samples were isochronally annealed at different temperature of 200, 400, 600, 700, 800, 900 and 1000 °C in air for a constant duration (2 h).

2.2. Experimental method

XRD analysis was performed by using Cu-K_α radiation (λ=1.5406 Å) on "Bruker D8" X-ray diffractometer. Si crystal was used as an external standard to correct for the instrument line broadening. Data were collected from 20° to 80° (2θ) with a step size of 0.02°. There were no monochromators in the whole XRD system. Thus there occurred Cu-$K_{\alpha1}$ and Cu-$K_{\alpha2}$ radiation at the same time, and each Bragg reflect ion took place with slightly different diffraction angles. When the XRD data were processed, the contribution of Cu-$K_{\alpha2}$ was stripped by using Jade software and only the pure Cu-$K_{\alpha1}$ radiation was left. The average particle sizes were determined by Debye-Scherrer formula. The morphology of the samples was investigated by a Hitachi S-4800 field emission scanning electron microscope (SEM).

Positron annihilation lifetime spectroscopy (PALS) was performed using a conventional fast-fast coincidence system with a temporal resolution of about 280 ps. A ^{22}Na positron source with intensity of about 20 μCi was used. The positron source of ^{22}Na was sealed between two Kapton films. Each spectrum was collected with a total count of 1×10^6. During the measurement, the positron source was sandwiched between two identical sample pieces. The components of the positron annihilation in the source and Kapton films were carried out using Si single crystal as reference. The spectra were analyzed using an analysis software (LT, version 9)[32] based on the sum of the exponential decay curves given by the following equation:

$$-\frac{dn(t)}{dt} = \sum_i^n I_i\tau_i \exp(-\tau_i t)\,,\ \sum_i^n I_i = I \qquad (1)$$

Where $n(t)$ is that the positron is alive at time t after its birth and τ_i is the lifetime associated with a decay curve with its initial intensity, I_i. Two lifetime components τ_1, τ_2, and corresponding percentage intensities, I_1, I_2, were resolved in the case of the CuO nanoparticles samples.

Doppler broadening spectroscopy (DBS) was measured using a liquid-nitrogen cooled high-purity (HP)-Ge detector with an energy resolution of about 1.50 keV at 511 keV. The source is sandwiched between the sample pair similar to positron lifetime experiments. The DBS were characterized by shape (S) and wing (W) parameters, which are linked to the interaction of the electron-positron pair with low-momentum valance electrons and high-momentum core electrons, respectively. The S and W parameters were defined respectively as the ratio of the central region (511 ± 0.8 keV) and the wing region (511 ± 3.4 to 511 ± 6.8 keV) of the spectrum to the entire region of the spectrum.

3. Results and discussion

The XRD patterns for all the samples are showed in Figure 1(a). No peaks of impurity phases (Cu_2O or Cu) are detected in these XRD patterns. All diffraction peaks as the typical monoclinic structure of CuO are observed, which show that the experimental samples are located in the CuO stable region when annealing in the temperature ranging from 200 to 1000 °C for 2 h. The whole CuO planes are used to calculate the average grain size. The average grain size of the CuO samples, as is shown in Figure 1(b), is calculated from the full width at half maximum of their diffraction curves by using Debye-Scherrer formula[33], i.e.

$$D = K\lambda / \beta\cos\theta \qquad (2)$$

Where D is the particle size, K is the constant shape factor (taken as 0.89), λ is taken as the wavelength of X-ray radiation, β is the full width at half maximum (FWHM) of the XRD peak, and θ is the Bragg angle. The calculated average grain size of the as-pressured sample is about 36.8 ± 3 nm, which is consistent with the information provided by the vendors. The size of the CuO nanoparticles increases slowly with increasing annealing temperature in annealing temperature from 200 to 800 °C. Similar observations have also been reported by earlier literature[16]. When the samples are annealed from 800 to 1000 °C, the grain size increases from 43 to 60 nm accordingly.

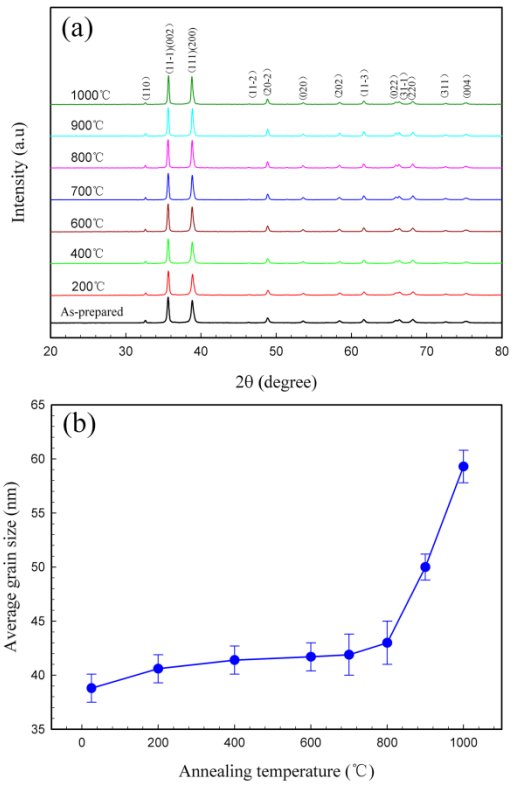

Figure 1. XRD patterns (a) and average grain size (b) of the CuO nanoparticles as a function of annealing temperature.

SEM images of CuO samples annealed at different temperatures are depicted in Figure 2. The testing part is the cross section of the CuO pellets. It can be seen that the CuO morphologies are not significantly changed below 800 °C. The CuO nanoparticles annealed at 800 °C began to aggregate into bigger particles, leading to an increase of grain size. These particles have a greater tendency to form clusters or aggregates when increasing the annealing temperature. However, due to limited resolution of SEM, the size of the CuO nanoparticles that assemble into micro-size cannot be estimated from the observed images, these grains have a very large average size (100–2500 nm) compared to that obtained by XRD analysis (40–60 nm). The crystallization of CuO nanoparticles is evidently improved with increasing the annealing temperature. This indicates that the grains are clusters of crystallites, consistent with results obtained previously[16, 19].

In order to further analyze the generation and recovery of defects located at grain surfaces or interfaces in CuO nanoparticles under isochronal annealing, we performed positron lifetime and Doppler broadening measurements. Figure 3(a) and Figure 3(b) show the positron lifetime parameters τ_1, τ_2, and their corresponding percentage intensities, I_1, I_2 as a function of annealing temperature in the case of the CuO nanoparticles samples. No meaningful change in two lifetimes (τ_1 and τ_2) and their corresponding percentage intensities (I_1 and I_2) are observed when the annealing temperature increases from 200 to 800 °C. Although the observed annihilation spectra in these samples appear to be two components, the simultaneous decrease in I_2 and τ_1 rules out the two-state trapping model which show a decrease in I_2 is accompanied by an increase in the τ_1 value[34]. Therefore, the short lifetime τ_1 cannot be exclusively attributed to positrons annihilated in the bulk of CuO. So, the short lifetime is associated with trapping at the bulk or mono-vacancy defects, and the long lifetime is assigned to trapped positrons in large vacancy clusters at the grain interfaces[29]. As seen in Figure 3, when the CuO nanoparticles is annealed at 200 °C, an increase in τ_1, τ_2 and I_1 while a decrease in I_2 has been observed. The defect states of the as-pressured sample (at room temperature) might be different from that of the sample sintered at 200 °C. When the CuO nanoparticles was annealed at 200 °C, the supply of small thermal energy conduced intragrain Cu and O vacancies to migrate towards the grain surfaces or interfaces. A rearrangement of nanoparticles would lead to the formation of more two-grain interfaces accompanied by a reduction in the number of three-grain junctions in the as-pressured sample without annealing. We observe that a small increase of τ_1, around 185 ps, is associated with positron trapping at vacancy-type defects in the two-grain interfaces, τ_2 increases from 308 to 360 ps due to positrons trapping at larger-size vacancy clusters in three-grain junctions[28], while the decrease of I_2 may be due to a reduction in the number of three-grain junctions. The bulk lifetime of about 169 ps in CuO was fixed according to the previous PALS studies[29, 35]. The value of τ_1 (~180 ps) is between the lifetime of positron annihilation in a bulk (169 ps) and a Cu mono-vacancy (230 ps)[29]. Hence, the value of τ_1 is attributed to a mixed contribution from the annihilation of trapped positrons in CuO bulk and mono-vacancies [28]. In the case of sample annealing at 1000 °C, with the largest average grain size 59.3 nm, I_2 decreases up to 2.2% and τ_1 results in a value of 165.8 ps which closes to the lifetime of positrons trapped at the CuO bulk. This likely indicates that positrons are mainly annihilated in the CuO bulk and V_{Cu} are absent in the CuO nanoparticles annealing at 1000 °C.

It is well-known that positrons were mainly trapped at neutrally or negatively charged (anion) vacancies and rarely trapped at positively charged (cation) vacancies since the probability of the positron annihilation with 1s electrons of oxygen was small owing to a strong Coulomb repulsion of the nucleus. The positron density concentrating near Cu-O bonds[36] and the shortest distance (1.95 Å) between Cu and O ions in a monoclinic cell of CuO were identified[37]. Therefore the effects of positron trapping at positively charged vacancies

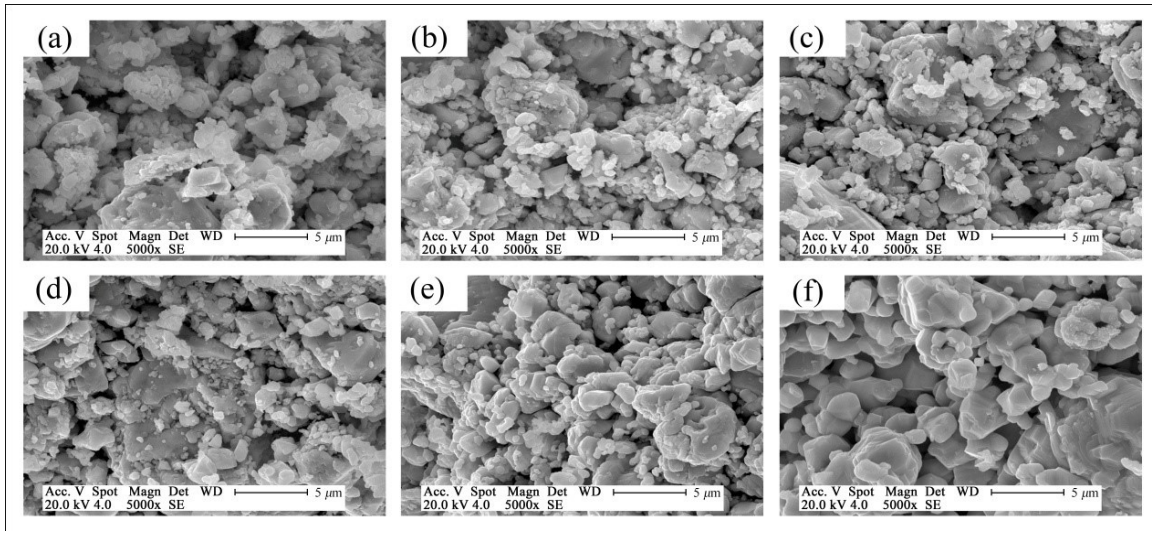

Figure 2. SEM images of CuO nanoparticles annealing at (a) room temperature (25 °C), (b) 400 °C, (c) 600 °C, (d) 700 °C, (e) 800 °C, and (f) 1000 °C.

cannot be neglected completely. A first-principles calculation of Wu et al.[12] found that only the V_{Cu}, V_O, Cu_i and O_{Cu} had one stable charge state V_{Cu}^{2-}, V_O^0, Cu_i^0 and O_{Cu}^{2-} in the whole range of the Fermi level in both *n*-type and *p*-type CuO in the O-rich environment, respectively. Meanwhile, the formation energy of Cu vacancies is lower than other type's defects, and the most stable defects, Cu vacancies, were also identified in CuO. Other vacancy-type defects found in CuO are V_O, but since the formation energy to V_O is around 3.5 eV, which is much larger than that of V_{Cu} (less than 1.0 eV), V_O may also be trapped positrons. The results of theoretical calculation and experiment in cuprate superconductors have proved that the dominant positron traps were presented by oxygen vacancy defects in the Cu-O planes[38-40]. It was also reported that open volumes which were mainly identified as anion vacancy defects existed in the grain interfaces in the CuO nanoceramics as well as the oxygen vacancy defects led to a decrease in the degree of Cu-O bond covalency studied by PAS[30]. Therefore, in present study, we consider that the effects of positron trapping at positively charged vacancies (V_O) cannot be neglected. Positrons may be annihilated in both V_{Cu} and V_O when the annealing temperatures varies from 200 - 800 °C. This will be analyzed in the following discussion of *W*-*S* plot.

The *S* and *W* parameters index the fraction of positron annihilating with the valence electrons and core electrons, respectively. The reduction in positron annihilation with core electrons is much more as compared to the valence electrons leading to the *S* parameter is higher than *W* parameter. Consequently, the data from DBS provides further insight on open volume defects (vacancies, vacancy clusters and voids). The *S* parameter reveals that the information of the size and concentration of defects in the different annihilation sites of solids[41] and can be correlated to the positron average lifetime (τ_a), which is calculated by the following equation:

$$\tau_a = \tau_1 I_1 + \tau_2 I_2 \quad (3)$$

The *S* parameter and τ_a as a function of annealing temperature are shown in Figure 4. It is seen that both *S* parameter and τ_a show a similar trend. The *S* parameter and τ_a decrease slightly with the annealing temperature from 200 to 800 °C and decrease rapidly above 800 °C. It can be concluded that the total concentration of interfacial defects reduces with the increase of grain size. Similar results were observed in ZnO nanoparticles studied by Sharma et al.[25].

Further discussion is from the set of *S* and *W* data plotted in the *W*-*S* plane which reveals the information about the overall defect types, as is shown in Figure. 5. It is interesting to observe that the (*W*, *S*) points distribute on two straight lines: first straight line segment from 200 to 800 °C and second straight line segment from 800 to 1000 °C. The straight line can be explained by the change in the concentration of the identical defect in the series samples[42]. It is indicated that the vacancy species are changed, producing two types of defects. As seen in Figure. 4(b), when the annealing

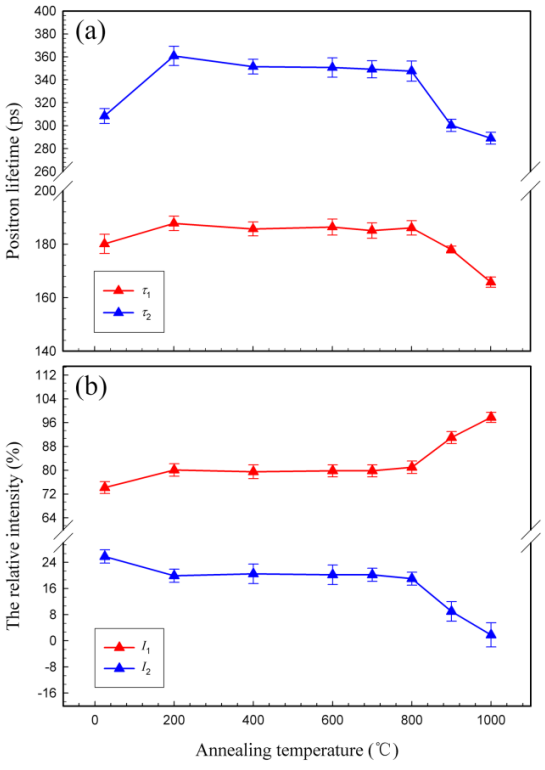

Figure 3. The CuO nanoparticles annealed at different temperature, (a) the positron lifetime values, τ_1, τ_2, (b) their corresponding percentage intensities, I_1, I_2.

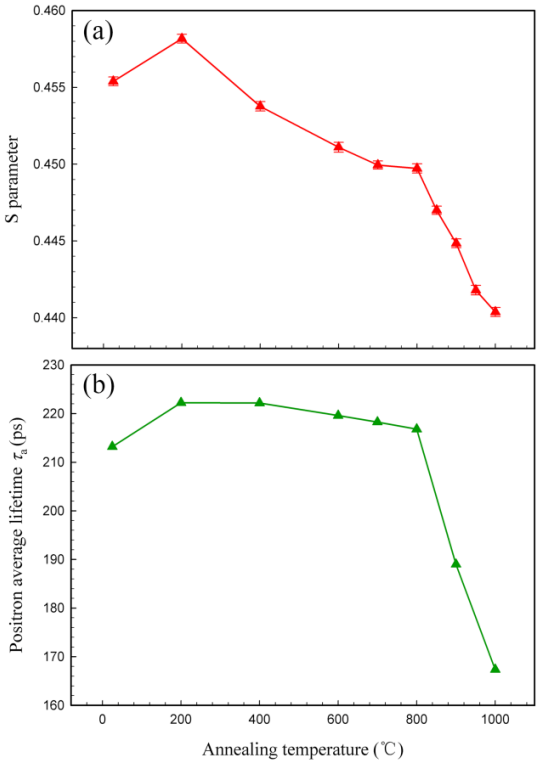

Figure 4. *S* parameter (a) and positron average lifetime (τ_a) (b) as a function of annealing temperature.

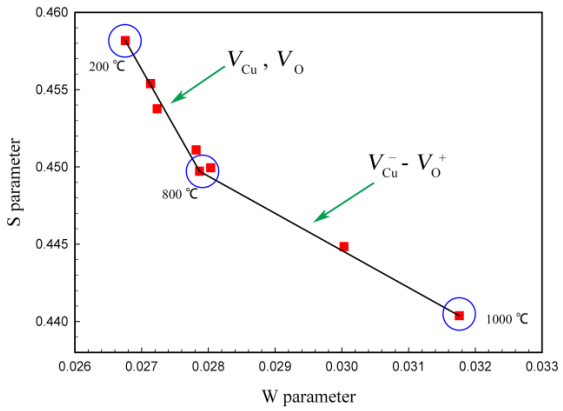

Figure 5. *W-S* plot for CuO nanoparticles

temperature varies from 200 to 800 °C, τ_2, with a value of about 350 ps, is essentially constant and larger than the lifetime of Cu mono-vacancies (230 ps). It can be understood that small-size Cu vacancies assemble and form the large-size Cu vacancy clusters at the grain interfaces. In addition, the effects of positron trapping at positively charged vacancies (V_O) cannot be also neglected when annealing below 800 °C. So, the first straight line is attributed to positrons annihilating in mono-vacancies (both V_{Cu} and V_O) and vacancy clusters at grains in CuO nanoparticles. When annealing above 800 °C, both τ_2 and I_2 begin to decrease rapidly while I_1 increases up to 97.8%. In this case, since the two trapping model is not suitable for explaining the behavior of positron annihilation parameters, a new complex structure of defects may be formed. Cruz et al.[43] identified that oxygen vacancies existed in Cu_2O single crystals annealing in air atmosphere at 923 °C in the stable region of the CuO phase as well as a lifetime of 320 ± 40 ps was attributed to positrons trapped at $V_{Cu}^- - V_O^+$ complexes. In present experiment, the value of τ_2 is close to the lifetime of the $V_{Cu}^- - V_O^+$ complexes (320 ± 40 ps), therefore, it is suggested that $V_{Cu}^- - V_O^+$ complexes at the grain interfaces may be formed due to fast diffusion of V_{Cu} and V_O when annealing above 800 °C, together with aggregates and growth of CuO nanoparticles. It can be concluded that when annealing temperature below 800 °C (first straight line segment of Figure 5), positrons are mainly annihilated in mono-vacancies (V_{Cu}, V_O) and vacancy clusters, while some positrons may annihilate in $V_{Cu}^- - V_O^+$ complexes above 800 °C (second straight line segment of Figure 5). Further work is needed to study the different annealing environment of CuO nanoparticles.

4. Conclusions

The microstructure and defects of CuO nanoparticles under isochronal annealing were studied by XRD, SEM and PAS. XRD results indicated that the average grain sizes of CuO nanoparticles varied from 40 to 60 nm. The crystallite of CuO nanoparticles grew slowly below 800 °C, and then nanoparticles increased with the annealing temperature up to 1000 °C. SEM images also indicated that the CuO nanoparticles annealed at 800 °C have began to aggregate into bigger particles, which were consistent with the growth of CuO nanoparticles seen in XRD patterns. PAS revealed that both *S* parameter and τ_a decreased slightly with the annealing temperature from 200 to 800 °C and decreased rapidly above 800 °C. The total concentration of interfacial defects in CuO nanoparticles reduced with the increase of grain size. PALS exhibited that the short lifetime, τ_1, which was attributed to a mixed contribution from the annihilation of trapped positrons in the bulk and mono-vacancies (V_{Cu}, V_O), and the long lifetime, τ_2, which was assigned to trapped positrons in large vacancy clusters below 800 °C. *W-S* plot of DBS found that the (*W*, *S*) points distributed on two different straight lines, which suggested that $V_{Cu}^- - V_O^+$ complexes were produced with the increase of grain size after annealing above 800 °C, positrons might annihilate at these complexes.

Acknowledgements

This work was supported by National Natural Science Foundation of China (11175136, 51071111, J1210061).

References

1. Heinemann M, Eifert B, Heiliger C. Band structure and phase stability of the copper oxides Cu_2O, CuO, and Cu_4O_3. *Physical Review B*. 2013;87(2):115111. DOI:http://dx.doi.org/10.1103/PhysRevB.87.115111
2. Kim H, Jin C, Park S, Kim S, Lee C. H2S gas sensing properties of bare and Pd-functionalized CuO nanorods. *Sensors and Actuators B: Chemical*. 2012; 161(1-3): 594-599.
3. Santos A, Yustos P, Quintanilla A, Ruiz G, Garcia-Ochoa F. Study of the copper leaching in the wet oxidation of phenol with CuO-based catalysts: causes and effects. *Applied Catalysis B: Environmental*. 2005;61(3-4):323-333. DOI: 10.1016/j.apcatb.2005.06.006
4. Carnes CL, Klabund KJ. The catalytic methanol synthesis over nanoparticle metal oxide catalysts. *Journal of Molecular Catalysis A: Chemical*. 2003; 194(1-2): 227-236.
5. Pendashteh A, Mousavi MF, Rahmanifar MS. Fabrication of anchored copper oxide nanoparticles on graphene oxide nanosheets via an electrostatic coprecipitation and its application as supercapacitor. *Electrochimica Acta*. 2013; 88:347-357. DOI:10.1016/j.electacta.2012.10.088
6. Dubal DP, Dhawale DS, Salunkhe RR, Jamdade VS, Lokhande CD. Fabrication of copper oxide multilayer nanosheets for supercapacitor application. *Journal of Alloys and Compounds*. 2010;492(1-2):26-36. DOI: 10.1016/j.jallcom.2009.11.149
7. Mostovshchikova EV, Gizhevskii BA, Loshkareva NN, Galakhov VR, Naumov SV, Ponosov YS, et al. Infrared and X-ray absorption spectra of Cu2O and CuO nanoceramics. *Solid State Phenomena*. 2012;190:683-686. DOI 10.4028/www.scientific.net/SSP.190.683
8. Sahay R, Suresh Kumar P, Aravindan V, Sundaramurthy J, Chui Ling W, Mhaisalkar SG, et al. High aspect ratio electrospun cuo nanofibers as anode material for lithium-ion batteries with superior cycleability. *The Journal of Physical Chemistry C*. 2012;116(34):18087-18092. DOI: 10.1021/jp3053949
9. Sahay R, Sundaramurthy J, Suresh Kumar P, Thavasi V, Mhaisalkar SG, Ramakrishna S. Synthesis and characterization

of CuO nanofibers, and investigation for its suitability as blocking layer in ZnO NPs based dye sensitized solar cell and as photocatalyst in organic dye degradation. *Journal of Solid State Chemistry*. 2012;186:261-267.

10. Hsieh CT, Chen JM, Lin HH, Shih HC. Field emission from various CuO nanostructures. *Applied Physics Letters*. 2003;83(16):3383-3385.
11. Wu D. *A first-principles study on bulk copper oxide: electronic structures and native point defects* [Dissertation]. Arlington: University of Texas; 2005.
12. Wu D, Zhang Q, Tao M. LSDA+Ustudy of cupric oxide: Electronic structure and native point defects. *Physical Review B*. 2006;73(23):235206. DOI:http://dx.doi.org/10.1103/PhysRevB.73.235206
13. Ray SC. Preparation of copper oxide thin film by the sol–gel-like dip technique and study of their structural and optical properties. *Solar Energy Materials and Solar Cells*. 2001;68(3-4):307-312.
14. Gao D, Zhang J, Zhu J, Qi J, Zhang Z, Sui W, et al. Vacancy-mediated magnetism in pure copper oxide nanoparticles. *Nanoscale Research Letters*. 2010;5(4): 769-772.
15. Shi S, Gao D, Xu Q, Yang Z, Xue D. Cu vacancies modulated the room temperature ferromagnetism in Cu2O/Cu nanoparticle composites. *CrystEngComm*. 2015;17(10):2118-2122. DOI: 10.1039/C4CE02542C
16. Rehman S, Mumtaz A, Hasanain SK. Size effects on the magnetic and optical properties of CuO nanoparticles. *Journal of Nanoparticle Research*. 2010;13(6): 2497-2507.
17. Borgohain K, Singh JB, Rama Rao MV, Shripathi T, Mahamuni S. Quantum size effects in CuO nanoparticles. *Physical Review B*. 2000;61(16):11093.
18. Krynetskiĭ IB, Gizhevskiĭ BA, Naumov SV, Kozlov EA. Size effect of the thermal expansion of nanostructural copper oxide. *Physics of the Solid State*. 2008;50(4):756-758.
19. Rao GN, Yao YD, Chen JW. Evolution of size, morphology, and magnetic properties of CuO nanoparticles by thermal annealing. *Journal of Applied Physics*. 2009;105(9):093901.
20. Schaefer HE, Würschum R, Birringer R, Gleiter H. Structure of nanometer-sized polycrystalline iron investigated by positron lifetime spectroscopy. *Physical Review B*. 1988;38(14):9545-9554.
21. Segers D, Petegem SV, Löffler JF, Swygenhoven HV, Wagner W, Dauwe C. Positron annihilation study of nanocrystalline iron. *Nanostructured Materials*. 1999;12(5-8):1059-1062. doi:10.1016/S0965-9773(99)00299-8
22. Eldrup MM, Sanders PG, Weertman JR. Positron annihilation study of the influence of grain size and purity on the annealing behaviour of nano-crystalline copper. *Materials Science Forum*. 1997;255:436-438. DOI: 10.4028/www.scientific.net/MSF.255-257.436
23. Eijt SW, van Veen AT, Schut H, Mijnarends PE, Denison AB, Barbiellini B, et al. Study of colloidal quantum-dot surfaces using an innovative thin-film positron 2D-ACAR method. *Nature Materials*. 2006;5(1):23-26. doi:10.1038/nmat1550
24. Weber MH, Lynn KG, Barbiellini B, Sterne PA, Denison AB. Direct observation of energy-gap scaling law in CdSe quantum dots with positrons. *Physical Review B*. 2002;66(4):041305(R). DOI: 10.1103/PhysRevB.66.041305
25. Sharma SK, Pujari PK, Sudarshan K, Dutta D, Mahapatra M, Godbole SV, et al. Positron annihilation studies in ZnO nanoparticles. *Solid State Communications*. 2009;149(13-14):550-554.
26. Puska MJ, Nieminen RM. Theory of positrons in solids and on solid surfaces. *Reviews of Modern Physics*. 1994;66(3):841-899.
27. Siegel RW. Positron annihilation spectroscopy. *Annual Review of Materials Science*. 1980;10:393-425. DOI: 10.1146/annurev.ms.10.080180.002141
28. Pareja R, Delacruz RM. Sintering of CuO investigated by positron lifetime spectroscopy. *Journal of Materials Science*. 1991;26(3):593-596.
29. Ameena F. *Defect studies in Cu-based P-type transparent conducting oxides*. [Dissertation]. Arlington: University of Texas; 2012.
30. Druzhkov AP, Gizhevskii BA, Arbuzov VL, Kozlov EA, Shalnov KV, Naumov SV, et al. Electronic and structural properties of micro-and nanometre-sized crystalline copper monoxide ceramics investigated by positron annihilation. *Journal of Physics: Condensed Matter*. 2002;14(34):7981-7990.
31. O'Keeffe M, Moore WJ. Thermodynamics of the formation and migration of defects in cuprous oxide. *The Journal of Chemical Physics*. 1962;36(11): 3009-3013. http://dx.doi.org/10.1063/1.1732418
32. Kansy J. Microcomputer program for analysis of positron annihilation lifetime spectra. *Nuclear Instruments and Methods in Physics Research Section A*. 1996; 374(2):235-244.
33. Warren BE. *X-ray Diffraction*. Massachusetts: Addison-Wesley; 1969.
34. Brandt W. Positron dynamics in solids. *Applied Physics*. 1974;5(1):1-23.
35. Nanchevaa N, Dochevaa P, Mishevab M. Defects in Cu and Cu–O films produced by reactive magnetron sputtering. *Materials Letters*. 1999;39(2): 81-85.
36. Turchi PE, Wachs AL, Wetzler KH, Kaiser JH, West RN, Jean YC, et al. Electron momentum density studies in high-Tc materials by positron annihilation spectroscopy: theory and experiment. *Journal of Physics: Condensed Matter*. 1990; 2(6):1635-1658.
37. Ghijsen J, Tjeng LH, Elp JV, Eskes H, Westerink J, Sawatzky GA, et al. Electronic structure of Cu_2O and CuO. *Physical Review B*. 1988;38(16): 11322-11330.
38. Stetten EC, Berko S, Li XS, Lee RR, Brynestad J, Singh D, et al. High Sensitivity of positrons to oxygen vacancies and to copper-oxygen chain Disorder in $YBa_2Cu_3O_{7-x}$. *Physical Review Letters*. 1988;60(21):198-2201.
39. Hermes H, Forster M, Schaefer HE. High-temperature equilibrium study of the oxygen-site occupancy in $YBa_2Cu_3O_{7-\delta}$ by positron annihilation. *Physical Review B*. 1991;43(13):10399-10404. DOI: 10.1103/PhysRevB.43.10399
40. McMullen T, Jena P, Khanna SN, Li Y, Jensen KO. Positron trapping at defects in copper oxide superconductors. *Physical Review B*. 1991;43(13):10422-10430.
41. Ferrell RA. Theory of positron annihilation in solids. *Reviews of Modern Physics*. 1956;28(3):308-337.
42. Clement M, de Nijs JM, Balk P, Schut H, van Veen A. Analysis of positron beam data by the combined use of the shape- and wing-parameters. *Journal of Applied Physics*. 1996;79(12):9029-9036.
43. de la Cruz RM, Pareja R, Diaz L, Garcia-Ramos JV. Annealing-induced positron trapping in Cu_2O single crystals. *Solid State Communications*. 1989;71(2):93-95. DOI: 10.1016/0038-1098(89)90441-9